Photostrictive Two-Dimensional Materials in the Monochalcogenide Family

Raad Haleoot,[1,2] Charles Paillard,[1,3] Thaneshwor P. Kaloni,[1] Mehrshad Mehboudi,[1] Bin Xu,[1,3] L. Bellaiche,[1,3] and Salvador Barraza-Lopez[1,*]

[1]*Department of Physics, University of Arkansas, Fayetteville, Arkansas 72701, USA*

[2]*Department of Physics at the College of Education, University of Mustansiriyah, Baghdad 10052, Iraq*

[3]*Institute for Nanoscience and Engineering, University of Arkansas, Fayetteville, Arkansas 72701, USA*

(Received 9 January 2017; published 30 May 2017)

Photostriction is predicted for group-IV monochalcogenide monolayers, two-dimensional ferroelectrics with rectangular unit cells (the lattice vector $\mathbf{a}_1$ is larger than $\mathbf{a}_2$) and an intrinsic dipole moment parallel to $\mathbf{a}_1$. Photostriction is found to be related to the structural change induced by a screened electric polarization (i.e., a converse piezoelectric effect) in photoexcited electronic states with either p_x or p_y (in-plane) orbital symmetry that leads to a compression of a_1 and a comparatively smaller increase of a_2 for a reduced unit cell area. The structural change documented here is 10 times larger than that observed in $BiFeO_3$, making monochalcogenide monolayers an ultimate platform for this effect. This structural modification should be observable under experimentally feasible densities of photexcited carriers on samples that have been grown already, having a potential usefulness for light-induced, remote mechano-optoelectronic applications.

DOI: 10.1103/PhysRevLett.118.227401

A truly novel optomechanical coupling in two-dimensional (2D) ferroelectric materials awaits to be discovered. Photostriction—the creation of nonthermal strain upon illumination [1–4]—has been well documented in three-dimensional ferroelectrics such as SbSI [5] and $BiFeO_3$ [6,7]. It has been suggested that photostriction is driven by the large voltage buildup caused by a photovoltaic effect and the resulting converse piezoelectricity [8], and it may be useful for applications such as remotely switchable memory devices [9] and light-induced actuators [10]. The earliest studied photostrictive material, SbSI, transitions from a ferroelectric onto a paraelectric at a critical temperature $T_c < 300$ K. As photostrictive effects are larger in the ferroelectric phase, T_c can be increased above 300 K on SbSI ceramics which have smaller domain sizes and display a nonuniform stoichiometry nevertheless. The photostriction response time increases with sample thickness, from a few picoseconds in ferroelectric films [11–17] up to a few seconds on bulk samples [5].

The growing interest in the interactions of light with 2D materials [18–21] makes a study of illumination leading to nontrivial structural deformations an interesting and timely endeavor. As long as a photoexcited state induces some amount of charge redistribution—which is a quite reasonable physical assumption—any material is expected to change shape as the structure is allowed to relieve the stress induced by the photoexcited carriers. Here, the surprising result is the rather large magnitude of such structural change for 2D ferroelectrics, which originates from an inverse piezoelectric effect upon illumination.

Two-dimensional ferroelectrics in the group-IV monochalcogenide monolayer family (GeS, GeSe, SnS, and SnSe, among others) [22–31] undergo a ferroelectric-to-paraelectric transition with a transition temperature that is tunable by atomic number [25]. Ferroelectricity originates from the noncentrosymmetric unit cells depicted in Fig. 1(a). Owing to structural symmetry, the electric dipole $\mathbf{P}_0$ is zero along the y and z directions, and finite along the x direction, as illustrated by two red horizontal arrows in Fig. 1(a), top view. The magnitude of P_0 is related to the projection of the vector joining atoms 1 and 2 (3 and 4) along the x axis, and to how delocalized the electronic charge is. The structural side view in Fig. 1(a) includes an electronic isosurface of 0.3 $e/\text{Å}^3$, intended to display delocalization qualitatively. The horizontal separation between group-IV and chalcogen atoms, and the degree of localization of electrons yields $P_0 =$ 2.77 and 2.06×10^{-10} C/m for SnS and SnSe, respectively. Lattice parameters for ground-state structures shown in Fig. 1(a) are $a_{1,0} = 4.3087$ Å and $a_{2,0} = 4.0786$ Å for SnS, and $a_{1,0} = 4.4038$ Å and $a_{2,0} = 4.2918$ Å for the SnSe monolayer.

Photostriction of SnS and SnSe is successfully predicted hereby, following the numerical approach proven to capture photostriction of $BiFeO_3$ [10] [photostriction of GeS is also demonstrated in the Supplemental Material (SM) [32]]. Screening of the electric dipole due to photoexcitation will be shown to be the main driver of the structural distortion. This effect could be readily observed in recent experimental setups such as the one in Ref. [26].

The challenge at hand and the computational approach are described first. Then, the two direct optical transitions to be employed to demonstrate the effect are motivated, and the anisotropic change of lattice parameters (photostriction) upon photoexcitation is documented. The decrease of the dipole moment and unit cell area seen in our numerical

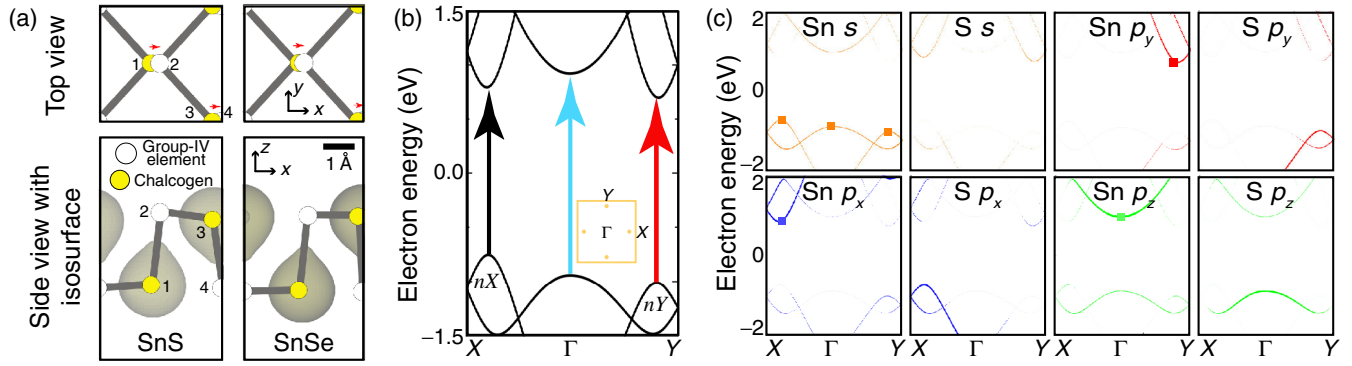

FIG. 1. (a) Unit cells for SnS and SnSe monolayers. Red arrows in the top views illustrate the direction of the electric dipole allowed by symmetry. A 0.3 $e/\text{Å}^3$ isosurface in the side view illustrates the delocalization of the electronic charge. (b) Band structure of SnS monolayer, displaying three direct optical transitions. A first Brillouin zone inset displays the $\pm nX$ and $\pm nY$ band edges as dots. (c) Orbital-resolved electronic structure of the SnS monolayer, with probability related to the observed line thickness. Optical transitions among valence band edge states with s symmetry (orange squares) and conduction band edge states with p_x, p_y, or p_z character at the nX, nY, or Γ band edges (highlighted by squares) are allowed by symmetry.

results are explained in terms of a photoinduced inverse piezoelectric effect and electronic pressure afterwards.

The concept is straightforward: one creates the effect of a direct optical transition at the valence and conduction band edges, allowing the structure to relax the forces created in the photoexcited state. Even though these materials are indirect band-gap semiconductors, the direct transitions shown by vertical arrows in Fig. 1(b) bring carriers onto the bottom of individual electron valleys. The two valleys near the corners of the first Brillouin zone are located at $0.390\mathbf{b}_1$ (nX) and $0.415\mathbf{b}_2$ (nY) for SnS [Fig. 1(b); $\mathbf{b}_1$ and $\mathbf{b}_2$ are reciprocal lattice vectors], and at similar locations for GeS and SnSe (see the SM [32]).

These direct transitions are unlike indirect transitions in materials like silicon or bulk dichalcogenides, where photoexcited electrons are never excited into a local valley and quickly release energy by coupling to lattice vibrations on their way into the band minima. In the present case, excited electrons face uphill energy bands in all directions due to the positive curvature of the local valleys, which may confine electrons sufficiently long for them to decay onto the valence band with non-negligible probability and preserving linear momentum.

Capturing photostriction requires approximations: specifically, the accuracy in forces needed to observe photostriction makes the Bethe-Salpeter approach [33,34]—the technique of choice for optical excitations in materials of reduced dimensionality—prohibitively expensive, and the same could be said of a time-dependent approach to the problem [35]. Indeed, photostriction under a density of photoexcited carriers n_c changes the lattice parameters $|\Delta a_i/a_{i,0}| \equiv |[a_i(n_c > 0) - a_{i,0}]|/a_{i,0}$ $(i = 1, 3)$ to within $10^{-5} - 10^{-4}$ in bulk samples [3], making for a prohibitively expensive optimization of the electron-hole-pair hosting structure [$a_{i,0} \equiv a_i(n_c = 0)$ here].

However, the recent discovery of ferroelectricity in monochalcogenide monolayers [25,26] gives an opportunity to extend this well-known effect into 2D materials, and the structural deformation in photoexcited monochalcogenide monolayers will be demonstrated using a technique [10] that successfully reproduces the experimentally observed photostriction of $BiFeO_3$ [36].

Görling formulated the interacting, photoexcited Hamiltonian as a model noninteracting DFT Hamiltonian [37], and the Δ-self-consistent-field (ΔSCF) method is a realization of Görling's approach that assumes a one-to-one correspondence between the excited states of a Kohn-Sham Hamiltonian and the real system [38]. It creates a population imbalance akin to that produced from illumination by depleting a finite number of electrons in the valence band and promoting them onto higher energy bands. ΔSCF calculations of excited states for systems with reduced dimensions abound (e.g., Refs. [39–41]), and the ΔSCF method as implemented in the ABINIT code [42] is employed to predict structural effects of direct optical transitions on ferroelectric monochalcogenide monolayers here. Calculations were performed on periodic structures with Garrity-Bennett-Rabe-Vanderbilt projected-augmented-wave [43] pseudopotentials [44] of the Perdew-Burke-Ernzerhof type [45], which are known to underestimate the electronic band gap. Nevertheless, additional corrections make it prohibitive to demonstrate the effect within computational constraints.

Figure 1(c) shows the electronic structure of SnS decomposed in states with s, p_x, p_y, or p_z orbital symmetry and belonging to a specific atomic species (Sn or S); projected band structures for GeS and SnSe, displaying similar trends, are provided in the SM [32]. Line thicknesses reflect the relative probability of finding a given orbital symmetry for a given band and chemical element. Optical transitions require nonzero matrix elements $\langle p_{i,c}|\mathbf{r}|s_v\rangle$ for wave functions with $|p_i\rangle$ symmetry in the conduction band and $|s\rangle$ symmetry in the valence band $(i = x, y, z)$. According to Fig. 1(c), the group-IV element

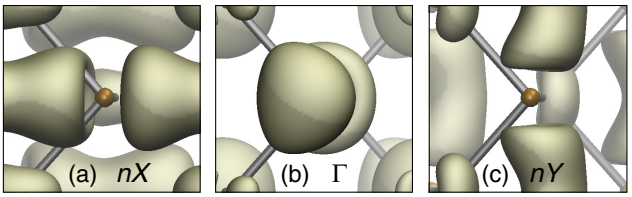

FIG. 2. SnS monolayer states at the (a) nX, (b) Γ, and (c) nY conduction local valley minima have p_x, p_z, and p_y orbital symmetries, respectively. Direct optical transitions at the nX and nY k points perturb in-plane orbitals and will lead to the largest photostriction.

(Sn) has an orbital s symmetry at the nX and nY valence band edges (as emphasized by the orange rectangles at such band edges; this is the case for GeS and SnSe, too—see the SM [32]). Similarly, a large probability is carried by Sn orbitals with p_x (p_y) symmetry at the nX (nY) conduction valley edge (the red rectangles). This way, the nonzero $\langle p_{i,c}|\mathbf{r}|s_v\rangle$ matrix element originates from a Sn *intra-atomic* direct optical transition with linearly polarized absorption band edges [28,46]. [Incidentally, one also notices that a direct optical transition at the Γ point would lead to an excited state with out-of-plane (p_z) symmetry.]

Illumination by pulsed laser sources can generate photoexcited carrier density fluences as high as $10^{13} - 10^{14}/\mathrm{cm}^2$ on MoS_2 samples [47]. After we discuss the k-point mesh employed in calculations, it will be shown that a much smaller density is needed for the effect being presently described to be experimentally achievable.

Considering spin-orbit coupling (SOC), a regular 2D mesh containing n_k^2 equally weighted k points yields a density of $n_c = 1/(n_k^2 A_0)$ charge carriers per band per k point per unit cell. The k-point mesh with $n_k = 41$—shown as an inset in Fig. 3(c)—allows us to create $n_c(n) = 2^2 n/(41^2 A_0) \simeq 1.3n \times 10^{12}/\mathrm{cm}^2$ excited charge carriers per band per unit cell. Here, the factor of 4 is due to the symmetry of the k-point mesh shown in the inset and because carriers from two bands immediately below the band gap are excited into two bands right above the band gap that are slightly split due to SOC; the dependence of n_c on $n = 0$, 1, 2, or 3 allows for a gradual increment of photoexcited carriers. Recalling that the photostriction of bulk samples results in $|\Delta a_i|/a_{i,0} \simeq 10^{-4} - 10^{-5}$ [3,10,36], a demanding relaxation limit for structural forces of 5×10^{-8} hartree/bohr and an energy cutoff of 40 hartree were employed in our calculations.

Figure 2 displays the orbital character of the conduction band at the nX, Γ, and nY k points prior to structural optimization. The orbital character of these transitions determines the strength of the photostrictive effect.

Indeed, Figs. 3(a) and 3(b) display a *decrease* of a_1 [$a_1(n_c > 0) < a_{1,0}$] and an *increase* of a_2 [$a_2(n_c > 0) > a_{2,0}$] for both SnS and SnSe monolayers. More specifically, the ratio $\Delta a_2(n_c)/\Delta a_1(n_c)$ is equal to -0.58 for the nX

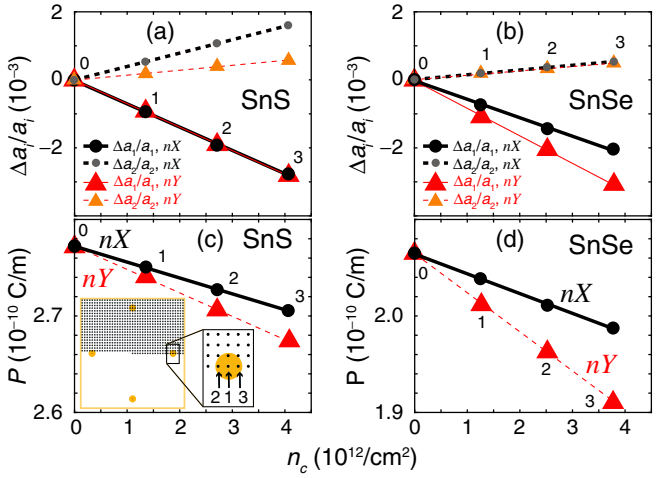

FIG. 3. Photostriction, a nonthermal change of a_1 and a_2 upon irradiation by light, is demonstrated for (a) SnS and (b) SnSe monolayers. The change on a_1 and a_2 is one order of magnitude larger than that for $BiFeO_3$, under experimentally accessible excited carrier densities. (c),(d) Photostriction decreases P. The inset in (c) shows the k-point mesh employed (the remainder of the Brillouin zone is included by symmetry), and the enlargement exemplifies three k points ($n = 1$, 2, 3) photoexcited around the nX point.

transition and -0.21 at the nY transition for SnS. In SnSe, $\Delta a_2(n_c)/\Delta a_1(n_c) = -0.26$ (nX) and -0.16 (nY). (For reference, Poisson ratios are 0.36 and 0.42 for SnS and SnSe, respectively [48].) In addition, a compression of the unit cell area A versus n_c ($A < A_0$) is found (see the SM [32]). Figures 3(a) and 3(b) contain the first prediction of photostrictive effects in 2D materials; they open a completely unexplored door for studies of coupled mechano-optoelectronic effects on 2D compounds.

Furthermore, the rather large change on a_1 and a_2 in Figs. 3(a) and 3(b) ($|\Delta a_i/a_{i,0}| \sim 10^{-3}$) (under experimentally accessible photoexcited charge carrier densities $n_c \sim 10^{12}/\mathrm{cm}^2$ [47]) is 1 to 2 orders of magnitude larger than that reported for bulk ferroelectrics, and hence quite encouraging: such large values of $\Delta a_i/a_{i,0}$ place these new photostrictive 2D materials in a class of their own. A similar photostriction for GeS (see the SM [32]) confirms the findings for SnS and SnSe, thus implying a generality of the effect on members of this material family for which $a_{1,0} \neq a_{2,0}$.

As indicated earlier, charge rearrangement is bound to occur upon photoexcitation, regardless of the numerical method employed (i.e., that in Refs. [33,34], in Ref. [35], or in the present one [37,38,42], which permits a comparatively small time-consuming tracking of the structural distortion). Local exciton wave functions on GeS and GeSe shown in Ref. [46] will also necessarily perturb the initial electric dipole and will lead to a structural distortion akin to the one shown here. Although the numerical estimates will depend on the method, the modification of the lattice structure with light is to be expected.

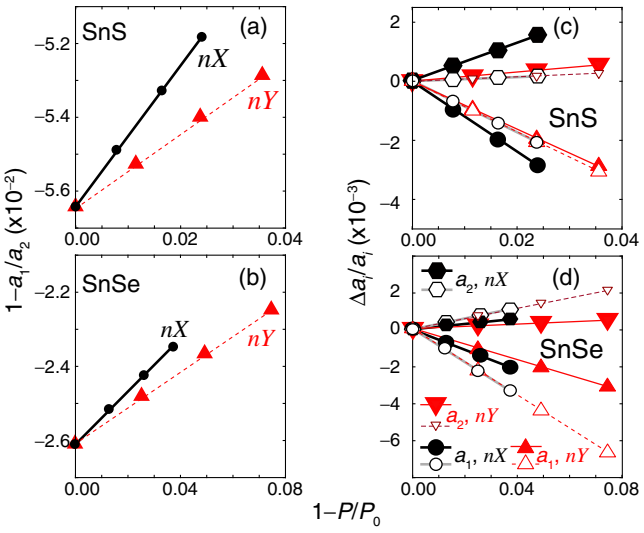

FIG. 4. (a),(b) The decrease of P is linearly dependent on the ratio a_1/a_2. (c),(d) The decrease of lattice parameters with P arises from an inverse piezoelectric effect, as calculated from Eq. (1) and shown as open symbols.

The effect of orbital symmetries on the magnitude of photostriction becomes manifest when testing a transition at the Γ point for states that are deeper within the conduction and valence bands. In that case, photostriction turns negligible (see the SM [32]): in-plane orbitals are naturally better at screening the electric dipole than out-of-plane orbitals that extend into the vacuum. In the same vein, the effect turns stronger than in the bulk because the structural change driven by screening in-plane orbitals is never counteracted from a (sturdier) 3D structure.

The reduction of P (obtained from Born effective charges) seen in Figs. 3(c) and 3(d) is related to the anisotropic change in lattice constants seen in Figs. 4(a) and 4(b) for SnS and SnSe, respectively. SnS and SnSe monolayers host an in-plane P parallel to the $\mathbf{a}_1$ lattice vector that becomes reduced as the ratio a_1/a_2 approaches unity [28]: this is why the polarization $P_0 \equiv P(n_c = 0) = 2.77 \times 10^{-10}$ C/m for SnS ($a_{1,0}/a_{2,0} = 1.056$) is larger than that for SnSe ($P_0 = 2.06 \times 10^{-10}$ C/m and $a_{1,0}/a_{2,0} = 1.026$) already and, within a given material, the reason for the thermally induced ferroelectric-to-paraelectric transition for a sudden change of the structural order parameter $a_{1,0}(T)/a_{2,0}(T)$ towards unity without illumination, where $P_0(T_c)$ goes all the way to zero [28,30] at the transition temperature T_c. Photostriction is a new (optical) handle to reduce a_1 and increase a_2, regardless of the valley edges being excited [nX, nY, or Γ].

We showed the tunability of a_1 and a_2 with chemistry [25] and temperature [28]. Presently, the remarkable tunability under illumination is to be understood from an inverse piezoelectric effect [10] as follows. In 2D, the dielectric susceptibility χ_i^{2D} and the dielectric tensor ϵ_i (both diagonal) are related as $\chi_i^{2D} = [(\epsilon_i - 1)/4\pi]L$ [49–51], where L is the vertical separation between (periodic) layers. This way, using the numerical change in polarization $P - P_0$ (which occurs only along the x axis) and considering the $mm2$ point symmetry of these compounds, lattice parameters a_i ($i = 1, 2$) must evolve as [49,52]

$$\frac{\Delta a_i}{a_{i,0}} = \frac{d_{i1}}{8\pi\epsilon_0\chi_1^{2D}}(P - P_0), \tag{1}$$

as represented by the open symbols in Figs. 4(c) and 4(d). χ_1^{2D} is taken as is from Ref. [49]—and expressed in angstroms—and relaxed-ion values for d_{i1} were taken from Ref. [48]; ϵ_0 is the permittivity of vacuum [53]. These predicted trends are on the same order of magnitude to the values of a_1 and a_2 determined upon a full optimization of the photoexcited structure, and they imply that photostriction is primarily produced by an inverse piezoelectric effect due to a dipole screening by the photoexcited charge carriers.

Note that the slope in Eq. (1) is independent of the valley being photoexcited (nX or nY), making the predicted values for $\Delta a_i/a_{i,0}$ lie upon the same straight line. The actual polarization is slightly different when exciting the nX or the nY valley.

Electronic or hole pressure may also produce slight differences in slope when exciting different valleys. Elongation of in-plane lattice vectors leads to positive stress. When let to relax, however, the material *contracts* back to its original structure. In general, any structure with positive stress will contract in response. Therefore, in a first approximation, the lattice also displays an elastic *response* (having a *negative* sign) given by

TABLE I. In-plane stress (in GPa) prior to structural relaxation arising from photoexcitation at the nX and nY points for $n_c(1)$. Note that $\Delta a_i/a_{i,0}$ ($i = 1, 2$) below must be scaled by 10^{-4}.

SnS				SnSe			
nX	nX	nY	nY	nX	nX	nY	nY
σ_{xx}	σ_{yy}	σ_{xx}	σ_{yy}	σ_{xx}	σ_{yy}	σ_{xx}	σ_{yy}
0.029	0.023	0.023	0.029	0.027	0.024	0.024	0.026
$\Delta a_1/a_{1,0}$	$\Delta a_2/a_{2,0}$	$\Delta a_1/a_{1,0}$	$\Delta a_2/a_{2,0}$	$\Delta a_1/a_{1,0}$	$\Delta a_2/a_{2,0}$	$\Delta a_1/a_{1,0}$	$\Delta a_2/a_{2,0}$
−8.3	0.5	−4.6	−1.9	−7.9	−0.3	−6.1	−1.3

$$\frac{\Delta a_i}{a_{i,0}} = C_{ij}^{-1}(-\sigma_j). \quad (2)$$

Using the elastic coefficients from Ref. [49] and the in-plane stress recorded in Table I for $n_c(1)$ from the initial photoexcited structure prior to any structural relaxation, we obtain changes of $\Delta a_i/a_{i,0}$ from Eq. (2) that are an order of magnitude smaller than those seen in Figs. 4(c) and 4(d). This way, the results from structural optimization shown in solid symbols in Figs. 4(c) and 4(d) have slopes that depend slightly on the electronic pressure (Eq. 2); these slopes are nevertheless dictated by the inverse piezoelectric effect (Eq. 1) predominantly, thus showing the relevance of ferroelectricity for this effect to occur in 2D materials.

The trends in Figs. 3 and 4 are similar to those for $BiFeO_3$, which implies similar mechanisms at play. Experimental realization of ferroelectric 2D monochalcogenide monolayers [26] (with no substantial depolarization fields due to size effects) enhances the present relevance of this work and brings optimism in that the unique effects here described will soon be experimentally verified.

In conclusion, photostriction of group-IV monochalcogenides has been predicted. Photostriction decreases the larger lattice vector a_1 and increases the smaller one a_2. It mainly arises from an inverse piezoelectric effect that reduces the dipole moment in the unit cell and contracts the lattice vector that is parallel to the electric dipole. These results continue to highlight unique properties of two-dimensional ferroelectrics and their potential usefulness for mechano-optoelectronic applications.

We thank H. Churchill, B. Hamad, and S. Sharifzadeh for discussions. R. H. was funded by The Higher Committee for Education Development of Iraq. T. P. K., M. M., and S. B.-L. were funded by the U.S. DOE (Grant No. DE-SC0016139). C. P. acknowledges the support from DARPA Grant No. HR0011-15-2-0038 (the MATRIX program). B. X. and L. B. acknowledge the U.S. AFOSR Grant No. FA9550-16-1-0065. Calculations were performed at SDSC's "Comet" (Grant No. XSEDE TG-PHY090002).

*sbarraza@uark.edu

[1] I. Tatsuzaki, K. Itoh, S. Ueda, and Y. Shindo, Phys. Rev. Lett. **17**, 198 (1966).
[2] V. M. Fridkin, I. I. Groshik, V. A. Lakhovizkaya, M. P. Mikhailov, and V. N. Nosov, Appl. Phys. Lett. **10**, 354 (1967).
[3] B. Kundys, Appl. Phys. Rev. **2**, 011301 (2015).
[4] C. Paillard, X. Bai, I. C. Infante, M. Guennou, G. Geneste, M. Alexe, J. Kreisel, and B. Dkhil, Adv. Mater. **28**, 5153 (2016).
[5] A. Dogan, P. Poosanaas, I. R. Abothu, S. Komarneni, and K. Uchino, J. Ceram. Soc. Jpn. **109**, 493 (2001).
[6] B. Kundys, M. Viret, D. Colson, and D. Kundys, Nat. Mater. **9**, 803 (2010).
[7] B. Kundys, M. Viret, C. Meny, V. Da Costa, D. Colson, and B. Doudin, Phys. Rev. B **85**, 092301 (2012).
[8] V. Fridkin, *Photoferroelectrics*, Springer Series in Solid-State Sciences, 1st ed., Vol. 9 (Springer, Berlin, 1979).
[9] V. Iurchuk *et al.*, Phys. Rev. Lett. **117**, 107403 (2016).
[10] C. Paillard, B. Xu, B. Dkhil, G. Geneste, and L. Bellaiche, Phys. Rev. Lett. **116**, 247401 (2016).
[11] Z. Jin, Y. Xu, Z. Zhang, X. Lin, G. Ma, Z. Cheng, and X. Wang, Appl. Phys. Lett. **101**, 242902 (2012).
[12] D. Daranciang *et al.*, Phys. Rev. Lett. **108**, 087601 (2012).
[13] H. Wen *et al.*, Phys. Rev. Lett. **110**, 037601 (2013).
[14] P. Ruello, T. Pezeril, S. Avanesyan, G. Vaudel, V. Gusev, I. C. Infante, and B. Dkhil, Appl. Phys. Lett. **100**, 212906 (2012).
[15] M. Lejman, G. Vaudel, I. Infante, P. Gemeiner, V. Gusev, B. Dkhil, and P. Ruello, Nat. Commun. **5**, 4301 (2014).
[16] D. Schick, M. Herzog, H. Wen, P. Chen, C. Adamo, P. Gaal, D. G. Schlom, P. G. Evans, Y. Li, and M. Bargheer, Phys. Rev. Lett. **112**, 097602 (2014).
[17] H. Wen, M. Sassi, Z. Luo, C. Adamo, D. G. Schlom, K. M. Rosso, and X. Zhang, Sci. Rep. **5**, 15098 (2015).
[18] A. Castellanos-Gomez, Nat. Photonics **10**, 202 (2016).
[19] X. Wang, A. M. Jones, K. L. Seyler, V. Tran, Y. Jia, H. Zhao, H. Wang, L. Yang, X. Xu, and F. Xia, Nat. Nanotechnol. **10**, 517 (2015).
[20] D. N. Basov, M. M. Fogler, and F. J. García de Abajo, Science, DOI: 10.1126/science.aag1992 (2016).
[21] D. N. Basov and M. M. Fogler, Nat. Nanotechnol. (to be published).
[22] G. A. Tritsaris, B. D. Malone, and E. Kaxiras, J. Appl. Phys. **113**, 233507 (2013).
[23] A. K. Singh and R. G. Hennig, Appl. Phys. Lett. **105**, 042103 (2014).
[24] Z. Zhu, J. Guan, D. Liu, and D. Tománek, ACS Nano **9**, 8284 (2015).
[25] M. Mehboudi, A. M. Dorio, W. Zhu, A. van der Zande, H. O. H. Churchill, A. A. Pacheco-Sanjuan, E. O. Harriss, P. Kumar, and S. Barraza-Lopez, Nano Lett. **16**, 1704 (2016).
[26] K. Chang *et al.*, Science **353**, 274 (2016).
[27] M. Wu and X. C. Zeng, Nano Lett. **16**, 3236 (2016).
[28] M. Mehboudi, B. M. Fregoso, Y. Yang, W. Zhu, A. van der Zande, J. Ferrer, L. Bellaiche, P. Kumar, and S. Barraza-Lopez, Phys. Rev. Lett. **117**, 246802 (2016).
[29] P. Z. Hanakata, A. Carvalho, D. K. Campbell, and H. S. Park, Phys. Rev. B **94**, 035304 (2016).
[30] R. Fei, W. Kang, and L. Yang, Phys. Rev. Lett. **117**, 097601 (2016).
[31] H. Wang and X. Qian, 2D Mater. **4**, 015042 (2017).
[32] See Supplemental Material at http://link.aps.org/supplemental/10.1103/PhysRevLett.118.227401 for a demonstration of photostriction on GeS and additional data on SnS and SnSe.
[33] L. Hedin, Phys. Rev. **139**, A796 (1965).
[34] M. S. Hybertsen and S. G. Louie, Phys. Rev. B **34**, 5390 (1986).
[35] C. A. Ullrich, *Time-Dependent Density-Functional Theory, Concepts and Applications*, 1st ed. (Oxford University Press, New York, 2012).
[36] B. Kundys, M. Viret, D. Colson, and D. O. Kundys, Nat. Mater. **9**, 803 (2010).

[37] A. Görling, Phys. Rev. A **59**, 3359 (1999).
[38] R. M. Martin, *Electronic Structure: Basic Theory and Practical Methods*, 1st ed. (Cambridge University Press, Cambridge, England, 2004).
[39] J. Gavnholt, T. Olsen, M. Engelund, and J. Schiøtz, Phys. Rev. B **78**, 075441 (2008).
[40] Y. Kitaoka, K. Nakamura, T. Akiyama, T. Ito, M. Weinert, and A. J. Freeman, Phys. Rev. B **87**, 205113 (2013).
[41] K. Nawa, Y. Kitaoka, K. Nakamura, H. Imamura, T. Akiyama, T. Ito, and M. Weinert, Phys. Rev. B **94**, 035136 (2016).
[42] X. Gonze *et al.*, Comput. Phys. Commun. **180**, 2582 (2009).
[43] P. E. Blöchl, Phys. Rev. B **50**, 17953 (1994).
[44] K. F. Garrity, J. W. Bennett, K. M. Rabe, and D. Vanderbilt, Comput. Mater. Sci. **81**, 446 (2014).
[45] J. P. Perdew, K. Burke, and M. Ernzerhof, Phys. Rev. Lett. **77**, 3865 (1996).
[46] L. C. Gomes, P. E. Trevisanutto, A. Carvalho, A. S. Rodin, and A. H. Castro Neto, Phys. Rev. B **94**, 155428 (2016).
[47] C. H. Lui, A. J. Frenzel, D. V. Pilon, Y.-H. Lee, X. Ling, G. M. Akselrod, J. Kong, and N. Gedik, Phys. Rev. Lett. **113**, 166801 (2014).
[48] R. Fei, W. Li, J. Li, and L. Yang, Appl. Phys. Lett. **107**, 173104 (2015).
[49] L. C. Gomes, A. Carvalho, and A. H. Castro Neto, Phys. Rev. B **92**, 214103 (2015).
[50] P. Cudazzo, I. V. Tokatly, and A. Rubio, Phys. Rev. B **84**, 085406 (2011).
[51] T. C. Berkelbach, M. S. Hybertsen, and D. R. Reichman, Phys. Rev. B **88**, 045318 (2013).
[52] J. Nye, *Physical Properties of Crystals* (Oxford University Press, Oxford, 1985).
[53] An additional factor of 2 multiplying χ arises from the length scale chosen for the vertical direction: a_3 in Ref. [48] and $a_3/2$ in Ref. [49].